eLife

Research Articles

Motor and Sensory Cortical Processing of Neural Oscillatory Activities revealed by Human Swallowing using Intracranial Electrodes

Subject Ares: Neuroscience

Hiroaki Hashimoto[a, b, c], Kazutaka Takahashi[d], Seiji Kameda[a], Fumiaki Yoshida[a, e], Hitoshi Maezawa[a], Satoru Oshino[f], Naoki Tani[f], Hui Ming Khoo[f], Takufumi Yanagisawa[f], Toshiki Yoshimine[c], Haruhiko Kishima[f], Masayuki Hirata[a, c, f ,*]

a. Department of Neurological Diagnosis and Restoration, Graduate School of Medicine, Osaka University, Yamadaoka 2-2, Suita, Osaka 565-0871, Japan.

b. Department of Neurosurgery, Otemae Hospital, Chuo-ku Otemae 1-5-34, Osaka, Osaka 540-0008, Japan

c. Endowed Research Department of Clinical Neuroengineering, Global Center for Medical Engineering and Informatics, Osaka University, Yamadaoka 2-2, Suita, Osaka 565-0871, Japan.

d. Department of Organismal Biology and Anatomy, University of Chicago, 1027 E 57th St, Chicago, IL 60637, USA.

e. Department of Physiology, Saga Medical School Faculty of Medicine, Saga University, Nabeshima 5-1-1, Saga, Saga 849-8501, Japan.

f. Department of Neurosurgery, Graduate School of Medicine, Osaka University, Yamadaoka 2-2, Suita, Osaka 565-0871, Japan.

* Masayuki Hirata, M.D., Ph.D. Specially-Appointed Professor

Department of Neurological Diagnosis and Restoration, Graduate School of Medicine, Osaka University, Yamadaoka 2-2, Suita, Osaka 565-0871, Japan.

Tel.: +81-6-6210-8429, Fax: +81-6-6210-8430

Email: mhirata@ndr.med.osaka-u.ac.jp

ORCID:

Hiroaki Hashimoto: https://orcid.org/0000-0003-4057-4466

Kazutaka Takahashi: https://orcid.org/0000-0001-7679-0430

Masayuki Hirata: https://orcid.org/0000-0002-9813-6728.

Keywords

swallowing, high gamma band, beta band, phase amplitude coupling, motor processing, Somatosensory processing, orofacial cortex, intracranial electrodes.

Author Contributions

M.H. designed the study. H.H. performed the experiments, assisted with the epileptic medical treatment, created the MATLAB program and analyzed the data, created all the figures and tables, and was primarily responsible for writing the manuscript. F.Y. H.M. and M.H. assisted in the acquisition of the measurements. S.K. developed some devices to help with the measurements. H.K., S.O., N.T., H.M.K. and M.H. performed the epilepsy surgery, and Ta.Ya. assisted with the epileptic medical treatment. M.H., K.T. and Ta.Ya advised H.H. on scientific matters. M.H. and K.T. revised the manuscript. To.Yo., H.K. and M.H. supervised the experiments and analyses. All authors reviewed the manuscript.

This file includes:

Main Text
Figures 1 to 9
Supporting information

Abstract

Swallowing is a unique movement because orchestration of voluntary and involuntary movement, and coordination between sensory input and motor output are indispensable. We hypothesized that neural mechanism of them were revealed by cortical oscillatory changes. Eight epileptic participants fitted with intracranial electrodes over the orofacial cortex were asked to swallow a water bolus, and cortical oscillatory changes were investigated. At the boundary time between voluntary and involuntary swallowing, high γ (75-150 Hz) power achieved the peak, and subsequently, the power decreased. High γ power increases (burst) were associated with both sensory input and motor output. However, phase-amplitude coupling (PAC) revealed that sensory-related coupling appeared during high γ-bursts, and motor-related coupling appeared before high γ-bursts. The peak of high γ power suggests switching of swallowing driving force from the cortex to the brain stem, and PAC findings suggest that motor-related coupling induces later motor-related high γ-activities representing endogenous neural processing.

Introduction

Swallowing is a unique movement because coordination of voluntary and involuntary movements is necessary for swallowing, which are executed by cooperation between motor output and somatosensory input. The cerebral cortex plays a crucial role in swallowing movements and is assumed to trigger swallowing and modulate the brain stem, and the central pattern generator (CPG) for swallowing is assumed to be in the brain stem in humans (Ertekin & Aydogdu, 2003). Thus, the swallowing movement is divided into two components, voluntary movement and involuntary movement (Jean, 2001). Oropharyngeal somatosensory input is crucial to swallowing (Lowell et al., 2008; Teismann et al., 2007), and there is a close relationship between oropharyngeal somatosensory input and swallowing-related motor output (Gow et al., 2004). As soon as things are placed into the mouth, we rapidly judge whether they are food items or not.

The neural correlates of human swallowing are partly revealed by noninvasive methods, such as electroencephalography (EEG) (Satow et al., 2004), positron emission tomography (PET) (Hamdy, Rothwell, et al., 1999), transcranial magnetic stimulation (TMS) (Hamdy et al., 1996), functional magnetic resonance imaging (fMRI) (Hamdy, Mikulis, et al., 1999; Martin et al., 2001), and magnetoencephalography (MEG) (Dziewas et al., 2003; Teismann et al., 2009). The orchestration between voluntary and involuntary movement, and somatosensory input and motor output are necessary for swallowing, however, low temporal resolution of noninvasive methods made difficult to reveal the neural processing of switching from voluntary to involuntary swallowing. Moreover, previous studies have mainly focused on either motor or somatosensory aspects, and studies dealing with both swallowing-related motor and swallowing-related somatosensory functions are rare (Furlong et al., 2004).

Neurophysiological recording techniques such as the electrocorticogram (ECoG) are appropriate to identify neural oscillatory changes up to high frequency bands. Moreover, the temporal resolution of ECoG is high. A few reports have focused on swallowing-related cerebral oscillatory changes using MEG (Dziewas et al., 2003; Furlong et al., 2004), but only frequency bands <50 Hz were mainly analyzed. High-frequency activities (high γ band, >50 Hz) is a key oscillation that reflects the neural processing of somatosensory, motor, and cognition (Canolty et al., 2006; Crone et al., 1998; Hashimoto et al., 2017; Hirata et al., 2002) and shows better functional localization than lower frequency activity (Crone et al., 1998; Hirata et al., 2002). Moreover, the amplitude of high γ activity is modulated by a phase of low-frequency oscillations (Canolty et al., 2006). The relationship describing the amplitude of high γ associated with the phase of low-frequency oscillations is known as phase-amplitude coupling (PAC) (Cohen, 2008). This PAC plays different functional roles in cortical processing, such as motor execution (Yanagisawa et al., 2012) and somatosensory processing (Lakatos et al., 2008). Swallowing-related high γ activity and PAC has not been clarified. Here, we hypothesized that using ECoG enabled us to record swallowing-related high γ activities with high temporal resolution, and high γ activities and PAC analyses may contribute to reveal both of

switching mechanism from voluntary to involuntary swallowing and differences between motor and somatosensory neural processing.

Results

We studied eight patients with intractable epilepsy (four males and four females, aged 15–51 years with mean age: 27.8 ± 11.6 y) (Supporting Table S1) who had no swallowing disturbances, as confirmed by medical interviews. These patients had undergone craniotomy for temporal placement of intracranial electrodes to identify epileptic foci. We selected grid electrodes (4×5 array) over the lateral portion of the central sulcus as orofacial electrodes for analysis (18.9 ± 1.8 electrodes, Supporting Table S1). We instructed the participants to swallow a 2-mL water bolus at their own pace without external cueing. A water bolus was injected into the mouth by an experimenter using a syringe.

The electroglottographs (EGGs) and a throat microphone were used to detect the swallowing onset time (Firmin et al., 1997). The peak EGG signals corresponds to the transition time from voluntary to involuntary swallowing (Kusuhara et al., 2004). We defined the peak of EGG as the onset time of swallowing (Supporting Fig. S1A, S1B). In addition, we confirmed that the detected swallowing onset time was consistent with water swallowing, not saliva swallowing, using a video recorded by our newly developed simple swallow-tracking system (Hashimoto et al., 2018) (Supporting Fig. S1C). Using this video, the time of mouth opening and water injection were also detected. We inserted three types of triggers including mouth, water, and swallowing, which corresponded to each detected time into the ECoG data. The number of each type of trigger was the same for a given participant (average: 33.5 ± 5.1 times, Supporting Table S1).

Representative Spatiotemporal Oscillatory Changes

The spatiotemporal oscillatory changes in a representative participant (Participant 1; P1) are shown in Figure 1. Averaged time-frequency maps around swallowing triggers from -4.5 to 2.0 s showed a high γ band (>50 Hz) power increase within about -3.5 to -2.0 s in the pre- and postcentral gyri (Fig. 1A, 1B). Simultaneously, the pre- and postcentral gyri also showed a decrease in the low-frequency band <50 Hz. Within -2.0 to 0 s, previous high γ activities disappeared and a new high γ power increase was observed in Channel (Ch) 9. After 0 s, the pre- and postcentral gyri showed power increase in the low-frequency band <50 Hz.

A series of power contour maps for the high γ band (75–150 Hz) and β band (13–30 Hz) were calculated using 0.5 s time-window every 0.5 s intervals from -4.5 to 2.5 s (Fig. 1C), and the power of each time epoch were normalized using -5.0 s time epoch power. The location where the large high γ power increase appeared

produced sequential changes. First, the large high γ power increase was observed in the pericentral gyri, especially for the postcentral gyrus during -4.0 to -1.5 s. Subsequently, the subcentral area, that is the narrow gyrus between the caudolateral extreme of the central sulcus and the Sylvian fissure, (Ch9) was the site where the large high γ power appeared during -1.0 to -0.5 s. Conversely, before 0 s, the β contour maps showed a power decrease in a wide area, especially for the precentral gyrus. After 0 s, the previous high γ increase disappeared and the β power increase was observed over the same wide area.

High γ and β band Contour Maps with Swallowing, Mouth, and Water Triggers

For each participant, an averaged power contour map of the high γ and β band was created with mouth, water, and swallowing triggers (Fig. 2). The time-window was 500 msec obtained from before and after 250 msec of the triggers. The power was normalized using the power calculated from the 500 msec mark during -1.0 to -0.5 s before the mouth triggers. The significant power increase was indicated as white filled circles and a significant power decrease was indicated as black filled circles (single-sided permutation test with Bonferroni correction, corrected $p < 0.05$).

We could observe a different spatial pattern of power increase (burst) in the high γ band within the three triggers. With the mouth trigger, a high γ burst was mainly observed in the precentral gyrus, and with the water trigger, the high γ burst was observed in the pericentral gyri, especially in the postcentral gyrus. For the swallowing motion, the tendency for high γ bursts appeared in the region along the Sylvian fissure including the subcentral area and the pars opercularis. Conversely for the β band, it was difficult to identify a different spatial pattern. The power decrease (attenuation) in the β band were widely observed for all three triggers.

Spatial Distribution of Electrodes showing Significant Power Changes related to Swallowing, Mouth, and Water Triggers

All electrodes that showed significant power burst or attenuation in each participant were plotted using the Montreal Neurological Institute (MNI) normalized brain for each trigger group (Fig. 3A). The electrodes attached to the right hemisphere were transposed to the left hemisphere. In the high γ band, the power increasing electrodes were plotted extensively in the water and swallowing group rather than the mouth group. In the β band, the power decreasing electrodes were plotted extensively across all groups. For all three groups, a significant high γ burst was observed, but the numbers of high γ burst electrodes were different within three groups. In the water and swallowing groups, the electrodes indicating high γ bursts were larger than those indicating no changes or high γ attenuation (Fig. 3B). In the swallowing group, the number of high γ bursts was significantly larger than other groups (the single-sided Wilcoxon signed-rank test with Bonferroni correction, corrected $p = 0.023$). In the β band, the number of attenuation electrodes was larger than that of the no change or burst electrodes. In the mouth and water groups, the number of β attenuation signals was significantly higher than the other two groups (single-sided

Wilcoxon signed-rank test with Bonferroni correction, $p < 0.05$) (Fig. 3B). This result showed that high γ burst and β attenuation were notably observed across all groups.

The number of high γ burst in the mouth group was significantly fewer than those in the water and swallowing group (single-sided Wilcoxon signed-rank test with Bonferroni correction, $p = 0.012$) (Fig. 3C). The number of β attenuation signals of the mouth group was largest but was not significant. The degree of high γ burst of the water group was largest but not significantly. In terms of the degree of β attenuation, the three groups were almost equivalent. These results indicated that a more extensive region showed swallowing-related high γ bursts, but the degree of high γ burst was larger when triggered by water injection, and the degree of β attenuation showed no changes within the three groups, although, mouth-associated β attenuation was observed in more extensive regions.

The top 25% of electrodes indicating a significant increase in high γ power or degree of β attenuation were plotted over the MNI brain (Fig. 3D). For the high γ burst, electrodes related to water injection were active in the lateral portion of the central sulcus, and electrodes related to swallowing were active in the regions along the Sylvian fissure. Electrodes related to mouth opening were found in the precentral gyrus and in the ventrolateral prefrontal cortex (VLPFC), but were no better localized than the other groups. In β attenuation, electrodes related to the mouth and water group were localized in the VLPFC, and the localization appeared to be less specific in the swallowing group. This result indicated that high γ activities were better localized rather than β activities, and the high γ localization might reflect differences in neural processing. The result seemed to show that the area indicating β attenuation corresponded to the area where mouth-related high γ bursts were observed. Then, we investigated the correlation between the β and high γ bands.

Correlation between β and High γ bands

Within the three triggers, using electrodes indicating significant β power attenuation, we calculated correlation coefficients between β and high γ normalized power. The time-window was 500 msec and consisted of 250 msec before and after the onset time of each trigger. In both the mouth and water groups, the correlation coefficients showed negative values, and had positive values in the swallowing group (Fig. 4A). However, there were no significant changes. Using the 100 msec time-window which moved in 50 msec intervals from -250 msec to 250 msec of each trigger, the correlation coefficients between β and high γ normalized power were calculated, and the electrodes indicating β power attenuation were sequentially plotted (Fig. 4B). In the swallowing group, the correlation coefficients were positive, and in the water group, about half of were negative. In the mouth group, only at the -50 msec interval, the correlation coefficient achieved significant negative values ($p = 0.032$) (Fig. 4C). These results indicated that electrodes showing lower β power achieved higher γ power immediately before the mouth opening time trigger. Next, we evaluated how dynamic power changed in related to each trigger.

Dynamic Oscillatory Changes related to Each Trigger

The top 25% of electrodes showing significant power decreased in the β band signals and increased in the high γ bands shown in Figure 3D were used to calculate the averaged dynamic power changes in each β and high γ band as electrodes associated with each trigger (Mouth-related electrodes (Mouth E), Water E, and Swallowing E). For each band, we used three electrode groups and three trigger groups to derive nine different power plots (Fig. 5A). Participants first opened their mouths and the water bolus was injected into it, and finally, swallowing occurred. Therefore, data obtained from the mouth trigger (Mouth T), water triggers (Water T), and swallowing trigger (Swallow T) were arranged in chronological order.

Around 0 s of the mouth trigger, only Mouth E showed a high γ burst. Around 0 s of the water trigger, Water E showed a notable high γ burst and this propagated to Mouth E and Swallow E. At 0 s of the swallow trigger, in Swallow E, the high γ burst reached the peak value. The 0 s of the swallowing trigger corresponded to the boundary between voluntary swallowing and involuntary swallowing. Therefore, our results showed that during voluntary swallowing, high γ activities were maintained up to the voluntary swallowing motion, and subsequently, the high γ activities decreased. In high γ activities, there were obvious differences in the types of high γ burst observed in combination of each trigger and each related-electrode. Conversely, β power showed similar patterns for each trigger. In the mouth trigger, all associated electrodes showed the same pattern, whereby β power was suppressed before 0 s. For water triggers, β power remained inhibited, and with swallowing triggers, β attenuation continued up to about 0.5 s, thereafter β power rebounded.

We compared the lead-time when β or high γ power began to change between each trigger with each related electrode (Fig. 5B). The lead-time of the high γ burst of the Swallow E was significantly earlier than that of the Mouth E (single-sided Wilcoxon signed-rank test with Bonferroni correction, $p = 0.031$). Even in the Water E, the beginning time of high γ burst preceded the 0 s of water triggers. For the mouth trigger, β attenuation preceded the high γ burst, but changes were not significant. We plotted sequential changes in correlation coefficients between β attenuation and high γ activities a few seconds before and after 0 s of swallowing or mouth triggers (Fig. 5C). The significant negative correlation coefficients ($p < 0.05$) were observed at -1.8 s of the swallowing trigger and at -1.25 s of the mouth trigger in each. These timings represented the time before each high γ burst appeared. In both the mouth and swallowing triggers, the results showed that a negative correlation appeared before the high γ burst.

To investigate β activities, we plotted the normalized β power changes from -1.5 s to 6 s of mouth triggers (Fig. 5D). The β power started to decrease at about –0.5 s, and the β attenuation at 0 s of mouth triggers was maintained up to 4 s, after which the β power rebounded. As mentioned above, at -0.05 s, a significant negative

correlation between β and high γ power was observed (Fig. 4B, 4C, 5C). Therefore, we used the β power of all electrodes at -0.05 s to investigate the correlation between β–β powers. The sequential correlation coefficients between the β power at -0.05 s and the β power at a specific time was shown (Fig. 5D). After the 0 s of the mouth trigger, during the β attenuation, a significant positive correlation was observed ($p < 0.05$ with Bonferroni correction). The results indicated that the β attenuation was induced by mouth opening and the continuous β attenuation was correlated to the mouth-related β attenuation.

Here, varying types of high γ activities were observed for each associated electrode group corresponding to the swallowing, mouth, and water triggers. Next, we used the PAC method to investigate the correlation between these high γ activities and low frequency activities.

PAC Features related to Mouth, Water, and Swallowing triggers

We used PAC analysis with the synchronization index (SI) (Cohen, 2008). The SI is a complex number; thus, we calculated the magnitude of the SI values, SIm. To calculate the SIm, we used the electrodes that showed the top 25% significant increases in high γ power changes (Fig. 3D). First, SIm values were calculated as a combination of lower frequency (2–30 Hz, 1 Hz bin) and higher frequency (76–150 Hz, 4 Hz bin) at a certain time (Fig. 6). For mouth T, at -1.2 s rather than 0 s, a significant SIm between θ (4–8 Hz) and high γ band were observed. For water T, at -0.6 s or 0 s, significant SIm between δ (2–4 Hz) and high γ band were observed. For swallow T, a high SIm between low β (13–20 Hz) and high γ band appeared at -1.4 s or -1.1 s. However, at 0 s, this high SIm disappeared and significant high SIm between δ and high γ band were observed at 0 s or 0.5 s.

Next, temporal SIm changes were investigated fixing high frequency at 75–150 Hz (Fig. 7). From -1.4 s to -0.8 s of mouth T, the SIm of the θ band had higher values and at -1.2 s, the high SIm values were significant. From -1.0 s to 0.4 s of water T, the SIm of the δ band had high values and at -0.6 s, the high SIm values were statistically significant. From -1.4 s to -0.7 s of the swallow T, high SIm values of the low β band were observed and at -1.4 s, -1.3 s and -1.1 s, higher SIm values were significant. From -0.2 s to 1.3 s of swallow T, the SIm of the δ band was high and at 0.3 s, a significant SIm was observed.

High γ power conditioned by the θ phase in mouth T, the δ phase in water T, and a low β phase in swallow T were presented within each of the 6 phase-bins (60° width) (Fig. 7D). In mouth T and swallow T, the time at the high SIm corresponded to the time before the high γ burst. Conversely, in water T, the time of the high SIm corresponded to the time of high γ burst. At the time of the appearance of the high SIm, each phase-conditioned high γ power signal was well separated.

To identify the lower frequency phase to which the high γ power amplitude was coupled during the high SIm appearance, we calculated the average lower frequency oscillation and the average phase-coupled high γ normalized power, within each of the 6 bins of the lower frequency phase (60° width), θ phase in mouth T, δ phase in water T, and low β phase in swallow T (Fig. 8). All lower frequency oscillations peaked at 0° with the trough at 180°. In mouth T, the lowest high γ power was observed at the trough of the θ oscillation (180°) (Fig. 8A), while, for the swallow T, the largest high γ power was observed at the trough of the lowest β oscillation (180°) (Fig. 8C). In water T, the largest high γ power was observed at the peak of the δ oscillation (0°) (Fig. 8B). Among the three triggers, the shapes of lower frequency oscillations were the same; however, the method by which the high γ power was conditioned by the lower frequency phase were different.

In mouth T and swallow T, significant coupling between θ or low β and high γ bands were observed before the onset of the high γ burst. Finally, we investigated the correlation between SIm values when significant coupling was observed and high γ power at specific times using all electrodes (Fig. 9). In the mouth T, significant positive correlations between the θ–high γ SIm from -1.4 s to -0.8 s and the high γ power at -0.1 s were observed (p = 0.046). In the swallow T, a significant positive correlation between the low β–high γ SIm from -1.4 s to -0.7 s and high γ power at -0.05 s was observed (p = 0.039) (Fig. 9A). Sequential correlation coefficients between SIm during above time and high γ power at certain times are presented simultaneously using high γ normalize power plotting (Fig. 9B). Within mouth T, at -1.0, -0.45, -0.1, 0.45 and 0.5 s, a significant positive correlation ($p < 0.05$) was observed, and especially at -0.1 s, the high γ burst was also observed. Within the swallow T, at -0.3, -0.25 and -0.05 s, a significant positive correlation ($p < 0.05$) was observed, and simultaneously, a high γ burst was also observed. This result indicated that the higher SIm the electrodes recorded, then the larger the high γ burst the electrodes could achieve later.

Discussion

This human ECoGs study was the first to investigate orofacial cortical oscillatory changes up to the high γ band associated with motor and somatosensory neural processing invoked by a swallowing task. We analyzed the ECoG data with three triggers corresponding to the time when the participant's mouth was opened, a water bolus was injected into the mouth, and when the bolus was swallowed. Mouth opening (Mouth T) and swallowing (Swallow T) represent motor output movement of efferent neural activities, and water injection (Water T) represents a somatosensory input of afferent neural activities. We demonstrated that different neural activities were observed between the high γ band and lower frequency bands, especially for the β band. High γ burst and β attenuation were observed to be associated with mouth opening, water injection and swallowing, however, the distribution of high γ burst activity was more focal than that of β attenuation. The distribution of β attenuation was diffuse and extensive. High γ activities generally show more focal spatiotemporal distributions than lower

frequency activities (Crone et al., 1998). Analyses based on mouth-related, water-related, and swallowing-related triggers showed distinct high γ burst activity. Mouth-related high γ bursts were observed in the precentral gyrus and the VLPFC, and water-related high γ bursts were observed in the lateral portion along the central sulcus. Swallowing-related high γ bursts were observed in regions along the Sylvian fissure, including the subcentral area (Brodmann's areas; BA 43) and the frontal operculum (BA 44). The swallowing-related high γ bursts achieved the peak at the boundary time between voluntary and involuntary swallowing, therefore, we inferred that this power peak represented the switching of the swallowing driving force from the cortex to the brain stem. Next, to investigate the relationship between high- and low-frequency bands, we used the PAC method. The high γ bursts associated with somatosensory input were coupled with the δ band on increasing power. However, the high γ bursts associated with motor output were coupled with the lower frequency bands before increases in power (θ band with mouth-opening and low β band with swallowing). The motor-related coupling before the high γ burst showed a positive correlation with a subsequent high γ burst. Therefore, we inferred that this result reflected differences between somatosensory and motor neural processing, and motor-related coupling induces later motor-related high γ-activities.

Swallowing-associated high γ bursts were observed in the region along the Sylvian fissure, including the subcentral area (BA 43) and the frontal operculum (BA 44). Previous studies have reported that swallowing activated the subcentral area (Martin et al., 2004; Toogood et al., 2017) and the frontal operculum (Dziewas et al., 2003; Lowell et al., 2008). In our study, swallowing-associated high γ bursts achieved a peak at the onset time of swallowing triggers, and subsequently, the high γ power decreased. Swallowing is divided into three phases, namely, the oral, pharyngeal, and esophageal phases. The oral phase is voluntarily controlled, whereas the pharyngeal and esophageal phases are involuntarily controlled (Jean, 2001). We inserted the swallowing trigger at the boundary time between the oral and the pharyngeal phases (Kusuhara et al., 2004). Therefore, our swallowing triggers were inserted between the transition from voluntary to involuntary swallowing. In the present study, during the voluntary swallowing phase, the high γ bursts appeared; however, in conjunction with the completion of voluntary swallowing, the high γ activity also decreased. A previous ECoG study postulated that the cerebral cortex is involved in voluntary swallowing to a greater degree than in swallowing execution (Satow et al., 2004). Our finding that the high γ burst related to swallowing achieved a peak at the transition between voluntary and involuntary swallowing indicates a neural mechanism: the main drive for swallowing switches from the cerebral cortex to the brain stem. During the high γ decrease, the CPG of the brain stem might be activated.

β attenuation in the lateral pericentral gyri was induced by the tongue movement and by swallowing (Dziewas et al., 2003). In our study, β attenuation was invoked associated with mouth opening, and the β band attenuation remained until the completion of the swallowing movement. The negative correlation between β and high γ power bands were observed. This high γ burst with β attenuation was consistent with the ECoG findings (Crone et al.,

1998; Miller et al., 2007). High γ activities with reductions in β power were also induced by hand movements (Yanagisawa et al., 2011). The negative correlation between β and high γ power was also observed at the moment before the swallowing-associated high γ burst, and so, we inferred that both mouth-opening and swallowing-associated cortical neural processing belong to the same motor cortical network. Moreover, this β attenuation was released after the completion of the swallowing movement and β power increased. This re-activation is known as rebounded β (Salmelin et al., 1995).

Coupling related to mouth opening and swallowing was observed before the motor-related high γ burst. High γ activities related to hand movements were coupled with the α phase before the high γ increase (Yanagisawa et al., 2012), and a hold-and-release model of high γ amplitude was proposed, which indicated that strong coupling restricted the high γ activities and attenuation of the coupling releases the high γ activities. The high PAC state may suppress cortical information processing before the onset of movement, and its cessation may induce a shift to an active processing state (de Hemptinne et al., 2015). Our results show that the low and high frequency couplings related to mouth opening and swallowing were observed before the high γ burst. The couplings disappeared and a high γ power increased. Moreover, a positive correlation between coupling and later high γ power increasing were observed. We inferred that the low and high frequency coupling might be necessary for endogenous high γ burst associated with motor output, efferent neural activities. However, mouth opening- and swallowing-related oscillatory changes showed that the lower frequency phase coupled with the high γ amplitude differed. Moreover, in the previous study, the maximum value of the high γ amplitude related to hand movement was locked up to the trough (180°) of the α oscillation (Yanagisawa et al., 2012), and in our study, the high γ amplitude was locked up to the trough of the lower frequency oscillations, which was the minimum value related to mouth opening and the maximum value related to swallowing. These differences may indicate that mouth and swallowing-related cortical networks belong to different divisions belonging to a same motor cortical network.

In this study, the δ-high γ coupling associated with the water injection obtained high values at the same time as the high γ burst, but not before high γ burst. The somatosensory input-related high γ activities were exogenous neural activities, and the high γ activities increased simultaneously by coupling with the δ phase. This difference in the time when coupling occurs between motor output and somatosensory input may indicate that different neural processing mechanisms occur for efferent and afferent neural activities.

We found that a high γ burst was observed in the lateral pre- and postcentral gyri associated with the water injection stimulus. Tactile stimulation of the buccal mucosa activates the caudolateral primary somatosensory area (Miyaji et al., 2014). We expected that water-associated high γ bursts would appear after the water triggers, however, contrary to our expectation, the beginning of the water-related high γ burst was 0.9 s earlier than the onset time of the water trigger. The onset time of the water trigger corresponded to the time when water bolus

was injected by a syringe, which as fixed onto the lip. We inferred that the time lag was a result of the somatosensory input from the lip on which a syringe was placed.

Our study has several limitations. First, we focused only the orofacial cortex. Multiple cortices are activated during swallowing (Ertekin & Aydogdu, 2003), however our study could not demonstrate cortical activities other than in orofacial region. Second, in this study, we divided swallowing events into three parts (mouth opening, water injection, and swallowing), and discussed motor and somatosensory neural processing. For more precise analysis, we may need to treat these as separate events, i.e., mouth movement only, water injection into the mouth only, and swallowing only. Third, we inferred the switching mechanism of the swallowing-related main driving force from the cortex to the brain stem. In the future, we think that simultaneous recording of the cortex and the brain stem may be needed to reveal how the swallowing-related interaction between them works. Finally, the correlation between motor-related high γ power and PAC were demonstrated, however, the causation between them remain unclear.

In the conclusion, we demonstrated that swallowing-related high γ activities that achieved the peak at the boundary time between voluntary and involuntary swallowing might represent the switching process from the cortex to the brain stem for swallowing execution. Both motor output and somatosensory input evoked a high γ burst. The sensory- associated high γ burst were coupled with the δ phase at simultaneously with the high γ burst. Conversely, the motor-associated high γ bursts were coupled with a lower frequency phase before the high γ burst, and motor related-coupling were positively correlated with subsequent increases in high γ power. The PAC findings suggest that motor-related coupling induces later motor-related high γ-activities.

Materials and Methods

Materials and Methods

Participants. Eight patients with intractable epilepsy participated in this study (four males and four females, 15–51 years of age; mean age: 27.8 ± 11.6 y) (Supporting Table S1). All participants or their guardians were informed of the purpose and possible consequences of this study, and written informed consent was obtained. The present study was approved by the Ethics Committee of Osaka University Hospital (Nos. 08061, 16469).

Task. The experiments were performed approximately 1 week after surgical electrode placement when all participants fully recovered from surgery. The participants were asked to sit on a chair and to remain still, especially without moving their mouth. The participants then opened their mouths, and the examiner injected 2 mL of water into their mouths with a syringe. We requested that the participants keep the water bolus in their

412 mouths for approximately 1 s and then swallow it at their own pace without external cueing to prevent erroneous
413 volitional water swallowing (aspiration). After we confirmed that the participants had completed one swallowing
414 movement, the next water bolus was injected.
415
416 ***Swallowing monitoring.*** For noninvasive swallowing detection, we used an EGG, a microphone, and a motion-
417 tracking system. A laryngograph (Laryngograph Ltd, London, UK) was used as an EGG and recorded the neck
418 impedance changes associated with swallowing (Firmin et al., 1997). A pair of electrodes was placed on the neck
419 skin below the thyroid cartilage of the participants at an interelectrode center-to-center distance of 25 mm and
420 was held in place by an elastic band. Sounds of swallowing due to the bolus passing through the pharynx were
421 detected by a throat microphone (Kusuhara et al., 2004). We connected the throat microphone (Inkou mike; SH-
422 12iK, NANZU, Shizuoka, Japan) to the laryngograph to record the swallowing sounds. The shape of the
423 microphone was arched to fit around the participant's neck. The sampling rate of a laryngograph and a throat
424 microphone was 24,000 Hz. We captured the motion of the participants at 30 frames per second (fps) with the
425 motion-tracking system, which was newly developed by us using Kinect v2 (Microsoft, Redmond, Washington,
426 USA)(Hashimoto et al., 2018). The participants were seated facing Kinect v2, which was placed on a tripod at a
427 distance of one meter, and their mouth and throat movements were captured. An electric stimulator (NS-101;
428 Unique Medical, Tokyo, Japan) supplied digital synchronizing signals to the laryngograph and a 128-channel
429 digital EEG system. The signals made an LED light flash, which was captured by the RGB camera of Kinect v2.
430 The digital triggers and LED light flash enabled us to synchronize the multimodal data of an EGG, a microphone,
431 the video captured by our motion-tracking system, and an intracranial EEG (Supporting Fig. S1C). The
432 simultaneous recording of the EGG, microphone, and motion-tracking system enabled us to noninvasively monitor
433 the swallowing movements (Hashimoto et al., 2018). The RGB camera of the Kinect v2 device enabled us to the
434 detect time when the participants opened their mouths and when the water bolus was injected into the mouth.
435
436 ***Signal segmentation based on swallowing-related events.*** Swallowing activities caused swallowing-
437 associated impedance changes in the neck, and this impedance waveform was clearly associated with the
438 swallowing activities (Kusuhara et al., 2004). The laryngograph was used to identify reliable signals that relate to
439 swallowing (Firmin et al., 1997). The swallowing onset time was determined at the time when the impedance
440 waveform reached the peak. Swallowing sounds occurred frequently as the bolus of water passed through the
441 pharynx (Kusuhara et al., 2004), and their evaluation in conjunction with the EGG helped us to judge whether the
442 impedance change was caused by swallowing (Supporting Fig. S1A, S1B). Additionally, we confirmed that the
443 changes in impedance and sounds corresponded to water swallowing by using the video captured by our simple
444 swallow-tracking system (SSTS) (Hashimoto et al., 2018). We inserted swallowing triggers, which corresponded
445 to the swallowing onset time, into the ECoG data.
446

A previous study associated the neck impedance changes with the following swallowing stages: stage I (the oral stage), stage II (the pharyngeal stage), and stage III (the esophageal stage). The time of the EGG peak corresponded to the beginning of the pharyngeal stage (Kusuhara et al., 2004). Since the oral phase is voluntarily controlled and the pharyngeal and esophageal phases are involuntarily controlled (Jean, 2001), the swallowing onset time in this study corresponded to the transition time from voluntary swallowing to involuntary swallowing.

We could also detect the time when the participant opened his/her mouth and when the examiner injected water into the participants' mouth using the video captured by RGB camera of the SSTS (Supporting Fig. S1C). Mouth triggers and water triggers, which corresponded to different times, were also inserted into ECoG data (the number of each trigger is shown in Supporting Table S1).

ECoG electrodes. Different types of electrodes (Unique Medical Co. Ltd., Tokyo, Japan), including grid, strip, and depth types, were implanted in the subdural space during conventional craniotomy as a clinical epileptic surgery. For analysis, we chose planar-surface platinum grid electrodes (4×5 array) that were placed overt the lateral portion of the central sulcus (in all participants) (Fig. 2A). The number of total electrodes and selected grid electrodes in each participant are shown in Supporting Table S1. The diameter of the electrodes was 3 or 5 mm, and the interelectrode center-to-center distance was 5, 7, or 10 mm.

Electrode location. Preoperative structural magnetic resonance imaging (MRI) was obtained with a 1.5-T or 3.0-T MRI scanner, and postoperative computed tomography (CT) scans were acquired with the subdural electrodes in place. The CT images clearly showed the position of the electrodes with respect to the skull geometry. The implanted electrodes that were obtained from the CT images were overlaid onto the 3-dimensional brain renderings from the MRI volume that was created by FreeSurfer software (https://surfer.nmr.mgh.harvard.edu). We obtained the Montreal Neurological Institute (MNI) coordinates of the implanted electrodes with Brainstorm software (http://neuroimage.usc.edu/brainstorm/), which merged the preoperative MRI scans and postoperative CT scans. The location of the implanted electrodes that was visualized by Brainstorm was then confirmed by intraoperative photographs.

Data acquisition and preprocessing. The ECoG signals were measured with a 128-channel digital EEG system (EEG 2000; Nihon Kohden Corporation, Tokyo, Japan) and digitized at a sampling rate of 1000 Hz with a 0.3 to 333 Hz bandpass filter to prevent aliasing, and a 60-Hz notch filter to eliminate the AC line noise. Before any further processing, noisy electrodes were excluded from further analyses. In P1 and P3, two electrodes were excluded because of external noise contamination. Electrodes containing epileptic discharge were also excluded in P5 (5 electrodes). The ECoG signals were digitally re-referenced to a common average of implanted total electrodes in each participant. We analyzed the ECoG signals that were time-locked to the triggers.

Throughout the following analyses, a bandpass filter using a two-way least-squares finite impulse response (FIR) filter was applied to the ECoG signals. To prevent edge-effect artifacts, additional 250 msec data were attached to the initial and end points of the averaged signals. After band-passed filtering, the 250 msec extra data were excluded.

Spectral analyses. The ECoG signals were time-locked to each trigger and extracted. In Figure 1, a time-frequency analysis of the time-locked ECoG signals was performed using free EEG analysis software (EEGLAB version 14.1.2b, http://sccn.ucsd.edu/eeglab/) with a frequency range from 1–330 Hz and spectral power (in dB) calculated in 0.5-Hz bins with 200 data-points (from -5.0 to 2.5 s in every 33-msec window). The baseline for the time-frequency analysis was initially 0.5 s.
To create power contour maps, we divided the time-locked ECoG signals from -4.5 to 2.5 s into 15 intervals every 0.5 s. The power of each interval was calculated for each electrode with Hilbert transformation applied to band-passed waveforms including high γ band (75–150 Hz) and β band (13–30 Hz). A bandpass filter using a two-way least-squares finite impulse response (FIR) filter (pop_eegfiltnew.m from the EEGLAB toolbox) was applied to the time-locked ECoG signals. To prevent edge-effect artifacts, extra 250 msec of data collection were attached to the initial and end points of the time-locked ECoG signals. After band-passed filtering, the 250 msec extra data were excluded. We calculated the averaged power during 0.5 s time epoch in these two bands, and the averaged power was normalized with the mean and standard deviation (SD) of the power of the corresponding electrodes during -5.0 to -4.5 s of the swallowing triggers.

In Figure 2, the power contour maps were created from 0.5 s time-window consisting of before and after 250 msec of each trigger. The power of high γ band and β band were z-normalized with the mean and SD of the power during -1.0 to -0.5 s of the mouth triggers as baseline. Single-sided permutation tests were performed between trigger data and baseline data for each electrode in two frequency bands. Multiple comparisons were resolved by Bonferroni correction, and significant corrected p-values were <0.05.

Extraction of electrodes. Significant power increasing or decreasing electrodes (single-sided permutation tests with Bonferroni correction) are indicated as filled white or black circles in Fig. 2B. These electrodes were plotted over the MNI normalized brain using Brainstorm software (Fig. 3A). Significant electrode numbers or frequency power were compared by single-sided Wilcoxon signed-rank test with Bonferroni correction (Fig. 3B, 3C, 5B). The top 25% of electrodes indicating a significant high γ power increase (burst) or a significant β power decrease (attenuation) were extracted and plotted on the MNI normalized brain (Fig. 3D).

Correlation analysis of frequency power. We investigated the correlation between β and high γ band power using a linear regression model. We used MATLAB 2019b (MathWorks, Natick, MA, USA) for analysis described

herein and for the analysis described below. The power of two frequency bands were calculated by the Hilbert transformation and were applied to the band-passed waveforms obtained by 500-msec data-points consisting of before and after 250 msec of each trigger. Power was normalized by the power calculated using the data obtained from -1.0 to -0.5 s of mouth triggers. The correlation between β and high γ band of the electrodes which indicated significant reductions in β power were analyzed (Fig. 4A). Next, sequential correlation changes were investigated using 100 msec data-points at 50-msec intervals with each trigger. The correlation was analyzed using electrodes that indicated a decrease in β power (Fig. 4B, 4C, 5C). Sequential correlation changes between fixed β power at -0.05 s of mouth triggers and varying β power at specific time points from -1.5 s to 6.0 s of mouth triggers were investigated using all 151 electrodes (Fig. 5D).

Dynamic frequency power changes. The top 25% of electrodes indicating significant high γ power increases (burst) or significant β power reductions (attenuation) were defined as mouth-related electrodes (Mouth E), water-related electrodes (Water E) and swallowing-related electrodes (Swallow E) in each frequency band. From these electrodes, we obtained averaged waveforms relative to each trigger (mouth triggers: Mouth T, water triggers: Water T, swallowing triggers: Swallow T). For the acquisition of a power time series, the averaged time series were band-pass filtered, and the band-passed time series were subjected to Hilbert transformation. The power time series were normalized by the power from -1.0 s to -0.9 s of Mouth T. Averaged frequency power values were calculated from a 100 msec time-window which was shifted every 10 msec. The shifted 100 msec data-points were compared with 100 msec data-points from -1.0 s to -0.9 s of Mouth T using the permutation test. Multiple comparisons were resolved by a family-wise error (FWE)-corrected threshold (see below). The FWE-threshold is indicated as a red dashed line in Fig. 5A. In Fig.5A, power time series from -1.5 s to 0.5 s of Mouth T, from -1.5 s to 1.5 s of Water T and from -2.5 s to 2.5 s of Swallow T were calculated from each related-electrode. In Fig. 5D, the power time series from -1.5 s to 6.0 s of Mouth T were calculated from all electrodes.

PAC analyses. Trigger-related time-locked ECoG signal from high γ burst-associated electrodes were averaged. In low frequency band, the center of a bandpass filter were shifted every 1 Hz from 2 to 30 Hz, and the width of bandpass filter were ± 1 Hz. In the high frequency band, the center of a bandpass filter was shifted every 4 Hz from 76 to 150 Hz, and the width of bandpass filter were ± 35 Hz (Fig. 6). When the high frequency band was fixed as high γ band, 75–150 Hz bandpass filter was used (Fig. 7). Hilbert transformation was performed on the filtered signals to obtain the complex-valued analytic signals of each frequency band, $Z_\omega(t)$ (ω means the frequency band). The amplitude of each frequency band, $A_\omega(t)$, and the phase of each frequency band, $\varphi_\omega(t)$, was calculated from the complex-valued signals using Equation 1.

$$(1)\ \ Z_\omega(t) = A_\omega(t) \cdot \exp\left(i\,\phi_\omega(t)\right).$$

The synchronization index (SI) was used to measure the strength of PAC between the high frequency power amplitude and the low-frequency phases (Cohen, 2008). The power amplitude of the high frequency band was extracted as the squared magnitude of $Z_\gamma(t)$, the analytic signal calculated by the Hilbert transformation ($P_\gamma(t)$ = real $[Z_\gamma(t)]^2$ + image $[Z_\gamma(t)]^2$). For the main analysis, the power amplitude was averaged over a 1 s time-window (Fig. 6, 7), and the center of the time-window was shifted by 100 msec from -1.5 s to 0.5 s of Mouth T, from -1.0 s to 0.5 s of Water T and from -2.5 s to 1.5 s of Swallow T (Fig. 7). Phases of the high frequency power amplitude were also extracted from the Hilbert transformation ($\varphi_\gamma(t)$ = arctan (imag [Z ($P_\gamma(t)$)]/real[Z($P_\gamma(t)$)])). The phase time series, $\varphi_l(t)$, was obtained from the angle of the Hilbert transform of the bandpass filtered signal. SI was calculated using Equation 2.

$$\text{(2)} \qquad \mathrm{SI} = \frac{1}{n} \times \sum_{t=1}^{n} e^{i}[\,\phi_l(t) - \phi_\gamma(t)]$$

n is the number of time points during each 1 s time window. SI is a complex number; therefore, we used the magnitude of SI, referred to as SIm. SIm varies between 0 and 1, with 0 indicating that phases are completely desynchronized and 1 indicating that phase values are perfectly synchronized. For the phase-conditioned analysis, the lower frequency phase, consisting of θ band (4–8 Hz) with Mouth T, δ band (1–4 Hz) with Water T and low β band (13–20 Hz) with Swallow T, was divided into 6 intervals of 60° without overlaps: 0° ± 30°, 60° ± 30°, 120° ± 30°, 180° ± 30°, 240° ± 30°, and 300° ± 30°. High γ power was normalized by the high γ power from -1.0 s to -0.5 s of Mouth T. In a 1 s time window, high γ power amplitudes were averaged within each phase interval (Fig. 7D) (Yanagisawa et al., 2012). In the time when high SIm values were observed during from -1.4 s to -0.8 s of Mouth T, from -1.0 s to 0.4 s of Water T and from -1.4 s to -0.7 s of Swallow T, lower frequency oscillation and normalized high γ power amplitudes were averaged within each phase interval (Fig. 8).

Correlation analysis related to PAC. We investigated the correlation between SIm and high γ band power using linear regression model with all electrodes (total 151 electrodes). We used fixed SIm values, which were calculated from the duration when high SIm values were observed from -1.4 s to -0.8 s of Mouth T and from -1.4 s to -0.7 s of Swallow T. The lower frequency were θ band in the Mouth T and low β band in the Swallow T. High γ power was normalized by the high γ power from -1.0 s to -0.5 s of Mouth T, and 100 msec time-window centered at -0.1 s of Mouth T and at -0.05 s of Swallow T were used for calculation of high γ power (Fig. 9A). Next, sequential correlation and power changes were investigated using 100 msec data-points shifted every 50 msec from -1.4 s to 0.5 s of Mouth T or Swallow T (Fig. 9B).

Statistics. For statistical evaluation, we used single-sided Wilcoxon signed-rank test with Bonferroni correction (Fig. 3B, 3C, 5B). For the statistical evaluation of the power changes displayed as contour maps (Fig. 2B) or time-

series (Fig. 5A), we used a permutation test for the comparison between the active and baseline states (Maris & Oostenveld, 2007). In Fig. 2B, we applied a conservative Bonferroni correction to correct for multiple comparisons and used a corrected threshold of $p < 0.05$. In Fig. 5A, to correct for multiple comparisons, we used a familywise error (FWE)-corrected threshold. If one permutation test was done, we could obtain one distribution of differences. The maximum or minimum values of the distribution were stored, and the values at 95% of these distributions were taken as the FWE-corrected threshold, which is applied to the observed power time series.

For statistical assessment of SIm, the boot-strapping technique was used (Cohen, 2008). The phase time series of high frequency power amplitude is shifted in time by some random amount, and boot-strapping SIm (SImb) is calculated with the lower frequency phase. This procedure was repeated 1,000 times to create a distribution of SImb. The normalized SIm was calculated using the mean and SD of the distribution of SImb. Permutation p values were calculated by counting the number of SImbs above the observed SIm and dividing by 1,000. If the observed SIm exceeded 99% of the distribution of SImb, p values were less than 0.01, and it was deemed statistically significant. To correct for multiple comparisons, we used an FWE-corrected threshold. At each iteration in the distribution of SImb, the maximum values of SImb were stored, and the values at 95% of these distributions were taken as the FWE-corrected threshold, which is applied to the observed SIm(Cohen, 2014).

Acknowledgments

This work was supported by Japan Society for the Promotion of Science (JSPS) KAKENHI [Grant nos. JP26282165, JP18H04166, JP18K18366], by the Ministry of Internal Affairs and Communications, by a grant from the National Institute of Information and Communications Technology (NICT), and by a grant from the National Institute of Dental and Craniofacial Research (NIDCR)-RO1 DE023816.

Data availability. All data that were generated by or analyzed in this study are available from the corresponding authors upon reasonable request and after additional ethics approvals regarding the data provision to individual institutions.

Competing interests: The authors have no competing interests to declare.

References

Canolty, R. T., Edwards, E., Dalal, S. S., Soltani, M., Nagarajan, S. S., Kirsch, H. E., Berger, M. S., Barbaro, N. M., & Knight, R. T. (2006, Sep 15). High gamma power is phase-locked to theta oscillations in human neocortex. *Science, 313*(5793), 1626-1628. https://doi.org/10.1126/science.1128115

Cohen, M. X. (2008, Mar 15). Assessing transient cross-frequency coupling in EEG data. *J Neurosci Methods, 168*(2), 494-499. https://doi.org/10.1016/j.jneumeth.2007.10.012

Cohen, M. X. (2014). *Analyzing neural time series data: theory and practice*. MIT press.

Crone, N. E., Miglioretti, D. L., Gordon, B., & Lesser, R. P. (1998, Dec). Functional mapping of human sensorimotor cortex with electrocorticographic spectral analysis. II. Event-related synchronization in the gamma band. *Brain, 121 (Pt 12)*, 2301-2315.

de Hemptinne, C., Swann, N. C., Ostrem, J. L., Ryapolova-Webb, E. S., San Luciano, M., Galifianakis, N. B., & Starr, P. A. (2015, May). Therapeutic deep brain stimulation reduces cortical phase-amplitude coupling in Parkinson's disease. *Nature Neuroscience, 18*(5), 779-+. https://doi.org/10.1038/nn.3997

Dziewas, R., Soros, P., Ishii, R., Chau, W., Henningsen, H., Ringelstein, E. B., Knecht, S., & Pantev, C. (2003, Sep). Neuroimaging evidence for cortical involvement in the preparation and in the act of swallowing. *Neuroimage, 20*(1), 135-144. https://www.ncbi.nlm.nih.gov/pubmed/14527576

http://ac.els-cdn.com/S1053811903002854/1-s2.0-S1053811903002854-main.pdf?_tid=6acc34a6-2f0d-11e7-865e-00000aab0f02&acdnat=1493712213_963aeb9d1747aff1047791757f4abc9c

Ertekin, C., & Aydogdu, I. (2003). Neurophysiology of swallowing. *Clinical Neurophysiology, 114*(12), 2226-2244. https://doi.org/10.1016/s1388-2457(03)00237-2

Firmin, H., Reilly, S., & Fourcin, A. (1997). Non-invasive monitoring of reflexive swallowing. *Speech Hearing and Language, 10*, 171-184.

Furlong, P. L., Hobson, A. R., Aziz, Q., Barnes, G. R., Singh, K. D., Hillebrand, A., Thompson, D. G., & Hamdy, S. (2004, Aug). Dissociating the spatio-temporal characteristics of cortical neuronal activity associated with human volitional swallowing in the healthy adult brain. *Neuroimage, 22*(4), 1447-1455. https://doi.org/10.1016/j.neuroimage.2004.02.041

Gow, D., Hobson, A. R., Furlong, P., & Hamdy, S. (2004, Oct). Characterising the central mechanisms of sensory modulation in human swallowing motor cortex. *Clin Neurophysiol, 115*(10), 2382-2390. https://doi.org/10.1016/j.clinph.2004.05.017

Hamdy, S., Aziz, Q., Rothwell, J. C., Singh, K. D., Barlow, J., Hughes, D. G., Tallis, R. C., & Thompson, D. G. (1996, Nov). The cortical topography of human swallowing musculature in health and disease. *Nat Med, 2*(11), 1217-1224. https://www.ncbi.nlm.nih.gov/pubmed/8898748

http://www.nature.com/nm/journal/v2/n11/pdf/nm1196-1217.pdf

Hamdy, S., Mikulis, D. J., Crawley, A., Xue, S., Lau, H., Henry, S., & Diamant, N. E. (1999, Jul). Cortical activation during human volitional swallowing: an event-related fMRI study. *Am J Physiol, 277*(1 Pt 1), G219-225. https://www.ncbi.nlm.nih.gov/pubmed/10409170

http://ajpgi.physiology.org/content/ajpgi/277/1/G219.full.pdf

Hamdy, S., Rothwell, J. C., Brooks, D. J., Bailey, D., Aziz, Q., & Thompson, D. G. (1999, Apr). Identification of the cerebral loci processing human swallowing with H2(15)O PET activation. *J Neurophysiol, 81*(4), 1917-1926. https://www.ncbi.nlm.nih.gov/pubmed/10200226

http://jn.physiology.org/content/jn/81/4/1917.full.pdf

Hashimoto, H., Hasegawa, Y., Araki, T., Sugata, H., Yanagisawa, T., Yorifuji, S., & Hirata, M. (2017, Oct 27). Non-invasive detection of language-related prefrontal high gamma band activity with beamforming MEG. *Sci Rep, 7*(1), 14262. https://doi.org/10.1038/s41598-017-14452-3

Hashimoto, H., Hirata, M., Takahashi, K., Kameda, S., Katsuta, Y., Yoshida, F., Hattori, N., Yanagisawa, T., Palmer, J., Oshino, S., Yoshimine, T., & Kishima, H. (2018, 2018/03/23). Non-invasive quantification of human swallowing using a simple motion tracking system. *Scientific Reports, 8*(1), 5095. https://doi.org/10.1038/s41598-018-23486-0

Hirata, M., Kato, A., Taniguchi, M., Ninomiya, H., Cheyne, D., Robinson, S. E., Maruno, M., Kumura, E., Ishii, R., Hirabuki, N., Nakamura, H., & Yoshimine, T. (2002, Jan 25). Frequency-dependent spatial distribution of human somatosensory evoked neuromagnetic fields. *Neurosci Lett, 318*(2), 73-76. https://www.ncbi.nlm.nih.gov/pubmed/11796189

http://ac.els-cdn.com/S0304394001024831/1-s2.0-S0304394001024831-main.pdf?_tid=f1279276-9f1a-11e6-80e1-00000aab0f01&acdnat=1477885054_f82a4a6c1f5e75dba19e85b3c1e4df6f

Jean, A. (2001, Apr). Brain stem control of swallowing: neuronal network and cellular mechanisms. *Physiol Rev, 81*(2), 929-969. https://www.ncbi.nlm.nih.gov/pubmed/11274347

http://physrev.physiology.org/content/physrev/81/2/929.full.pdf

Kusuhara, T., Nakamura, T., Shirakawa, Y., Mori, K., Naomoto, Y., & Yamamoto, Y. (2004, Nov-Dec). Impedance pharyngography to assess swallowing function. *J Int Med Res, 32*(6), 608-616. http://www.ncbi.nlm.nih.gov/pubmed/15587754

http://imr.sagepub.com/content/32/6/608.full.pdf

Lakatos, P., Karmos, G., Mehta, A. D., Ulbert, I., & Schroeder, C. E. J. s. (2008). Entrainment of neuronal oscillations as a mechanism of attentional selection. *320*(5872), 110-113. http://science.sciencemag.org/content/320/5872/110.long

Lowell, S. Y., Poletto, C. J., Knorr-Chung, B. R., Reynolds, R. C., Simonyan, K., & Ludlow, C. L. (2008, Aug 1). Sensory stimulation activates both motor and sensory components of the swallowing system. *Neuroimage, 42*(1), 285-295. https://doi.org/10.1016/j.neuroimage.2008.04.234

Maris, E., & Oostenveld, R. (2007, Aug 15). Nonparametric statistical testing of EEG- and MEG-data. *J Neurosci Methods, 164*(1), 177-190. https://doi.org/10.1016/j.jneumeth.2007.03.024

Martin, R. E., Goodyear, B. G., Gati, J. S., & Menon, R. S. (2001, Feb). Cerebral cortical representation of automatic and volitional swallowing in humans. *J Neurophysiol, 85*(2), 938-950. https://www.ncbi.nlm.nih.gov/pubmed/11160524

http://jn.physiology.org/content/jn/85/2/938.full.pdf

Martin, R. E., MacIntosh, B. J., Smith, R. C., Barr, A. M., Stevens, T. K., Gati, J. S., & Menon, R. S. (2004, Oct). Cerebral areas processing swallowing and tongue movement are overlapping but distinct: a functional magnetic resonance imaging study. *J Neurophysiol, 92*(4), 2428-2443. https://doi.org/10.1152/jn.01144.2003

Miller, K. J., Leuthardt, E. C., Schalk, G., Rao, R. P., Anderson, N. R., Moran, D. W., Miller, J. W., & Ojemann, J. G. (2007, Feb 28). Spectral changes in cortical surface potentials during motor movement. *J Neurosci, 27*(9), 2424-2432. https://doi.org/27/9/2424 [pii]

10.1523/JNEUROSCI.3886-06.2007 [doi]

Miyaji, H., Hironaga, N., Umezaki, T., Hagiwara, K., Shigeto, H., Sawatsubashi, M., Tobimatsu, S., & Komune, S. (2014, Mar). Neuromagnetic detection of the laryngeal area: Sensory-evoked fields to air-puff stimulation. *Neuroimage, 88*, 162-169. https://doi.org/10.1016/j.neuroimage.2013.11.008

Salmelin, R., Hamalainen, M., Kajola, M., & Hari, R. (1995, Dec). Functional segregation of movement-related rhythmic activity in the human brain. *Neuroimage, 2*(4), 237-243. https://www.ncbi.nlm.nih.gov/pubmed/9343608

http://ac.els-cdn.com/S1053811985710312/1-s2.0-S1053811985710312-main.pdf?_tid=8ae377de-35ea-11e7-ae48-00000aab0f26&acdnat=1494466892_e977f504faba79f2c682e37b85dc23e9

Satow, T., Ikeda, A., Yamamoto, J., Begum, T., Thuy, D. H., Matsuhashi, M., Mima, T., Nagamine, T., Baba, K., Mihara, T., Inoue, Y., Miyamoto, S., Hashimoto, N., & Shibasaki, H. (2004, Aug). Role of primary sensorimotor cortex and supplementary motor area in volitional swallowing: a movement-related cortical potential study. *Am J Physiol Gastrointest Liver Physiol, 287*(2), G459-470. https://doi.org/10.1152/ajpgi.00323.2003

Teismann, I. K., Dziewas, R., Steinstraeter, O., & Pantev, C. (2009, Jan). Time-dependent hemispheric shift of the cortical control of volitional swallowing. *Hum Brain Mapp, 30*(1), 92-100. https://doi.org/10.1002/hbm.20488

Teismann, I. K., Steinstraeter, O., Stoeckigt, K., Suntrup, S., Wollbrink, A., Pantev, C., & Dziewas, R. (2007, Aug 02). Functional oropharyngeal sensory disruption interferes with the cortical control of swallowing. *BMC Neurosci, 8*, 62. https://doi.org/10.1186/1471-2202-8-62

Toogood, J. A., Smith, R. C., Stevens, T. K., Gati, J. S., Menon, R. S., Theurer, J., Weisz, S., Affoo, R. H., & Martin, R. E. (2017, Mar 30). Swallowing Preparation and Execution: Insights from a Delayed-Response Functional Magnetic Resonance Imaging (fMRI) Study. *Dysphagia*. https://doi.org/10.1007/s00455-017-9794-2

Yanagisawa, T., Hirata, M., Saitoh, Y., Goto, T., Kishima, H., Fukuma, R., Yokoi, H., Kamitani, Y., & Yoshimine, T. (2011, Jun). Real-time control of a prosthetic hand using human electrocorticography signals. *Journal of neurosurgery, 114*(6), 1715-1722. https://doi.org/10.3171/2011.1.Jns101421

Yanagisawa, T., Yamashita, O., Hirata, M., Kishima, H., Saitoh, Y., Goto, T., Yoshimine, T., & Kamitani, Y. (2012, Oct 31). Regulation of Motor Representation by Phase-Amplitude Coupling in the Sensorimotor Cortex. *Journal of Neuroscience, 32*(44), 15467-15475. https://doi.org/10.1523/Jneurosci.2929-12.2012

Figures

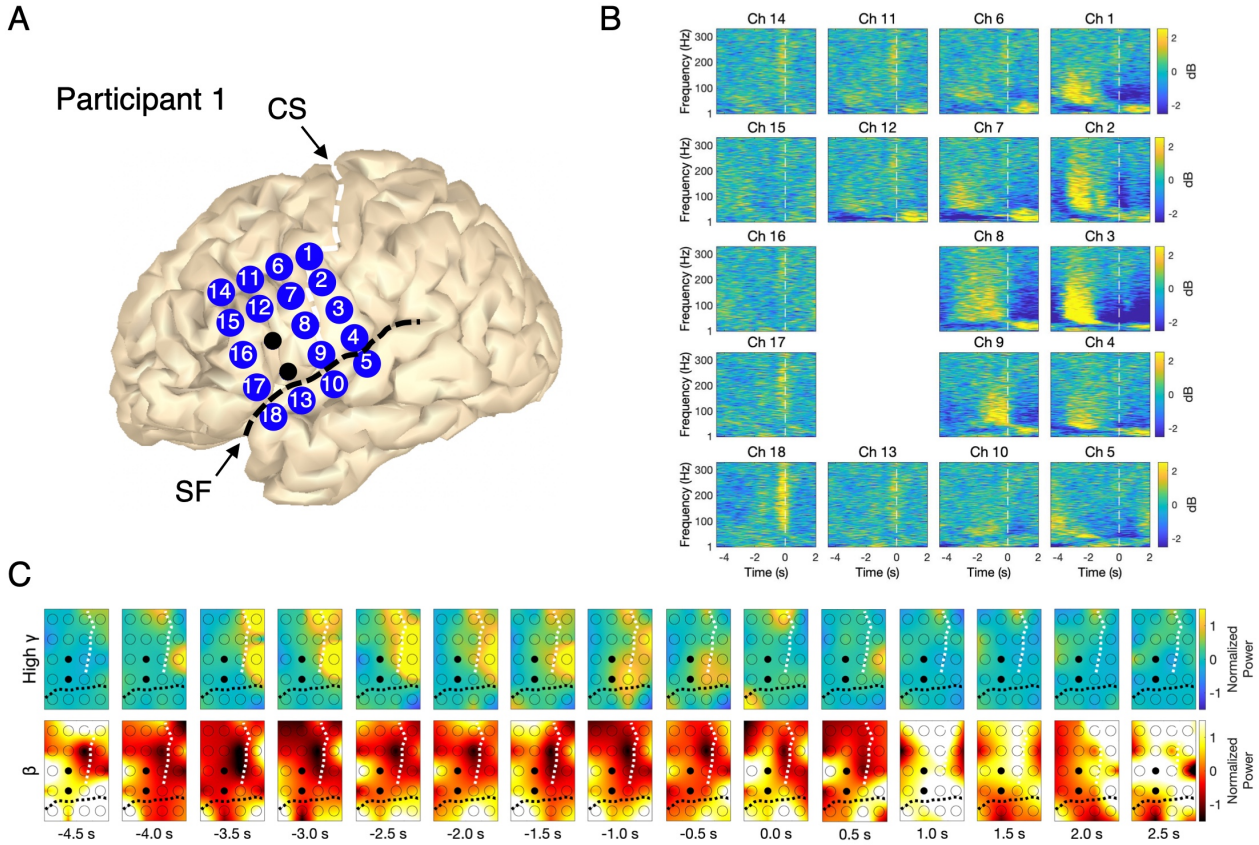

Figure 1. Temporal profiles of oscillatory changes associated with swallowing in P1. (A) The reconstructed MR images. The numbers correspond to the electrode numbers. (B) Averaged time-frequency maps are shown from -4.5 to 2.0 s around the swallowing trigger. These baselines of 0.5 s duration range from -5.0 to -4.5 s. High γ band power (>50 Hz) increases specific to swallowing appeared in Ch 9 attached to the subcentral area from -2.0 to 0 s. Within -3.5 to -2.0 s, the time-frequency plots from the pre and postcentral gyri showed high γ increases along with decreases in lower frequency band (< 50 Hz) power. After 0 s, the pre- and postcentral gyri showed the lower frequency power increase. (C) Contour maps of normalized power in high γ (75–150 Hz) and β (13–30 Hz) bands are shown from -4.5 to 2.5 s every 0.5 s interval around the swallowing trigger. The cortical areas in which the large power increased in the high γ band showed sequential changes. The electrode that showed the largest high γ power increases immediately before swallowing onset time (0 s) was Ch9, attached to the subcentral area. The two black electrodes were excluded because of severe noise contamination. The central sulcus (CS) and the Sylvian fissure (SF) are indicated by the white and black dashed lines in each.

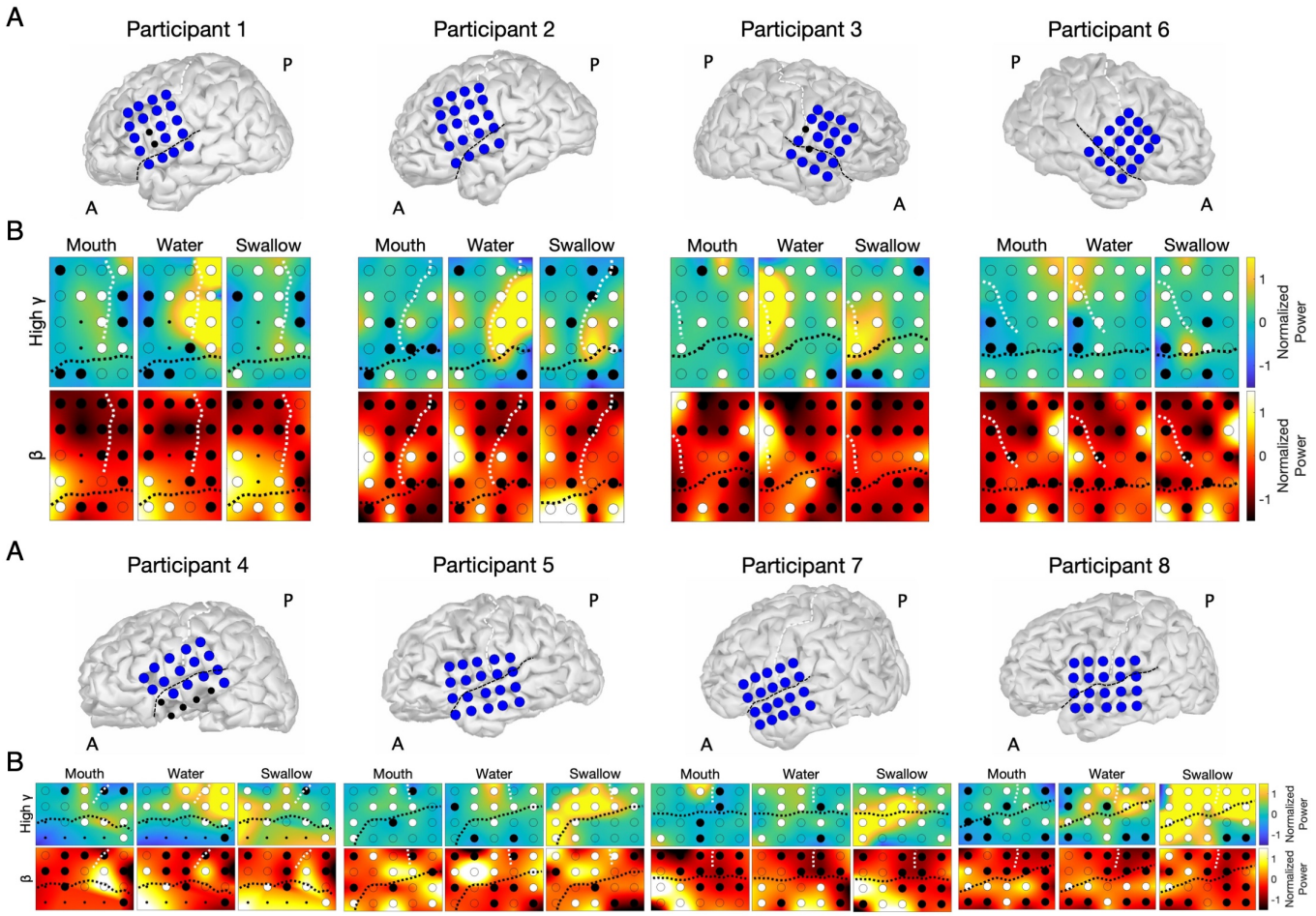

Figure 2. Power contour maps at mouth, water, and swallowing triggers in high γ and β band. (A) The reconstructed MR images for all participants. (B) The upper columns indicate high γ contour maps and the lower columns indicate β contour maps. Significant power burst was indicated as white filled circles, and significant power attenuation was indicated as black filled circles (Single-sided permutation test with Bonferroni correction, corrected $p < 0.05$). Excluded electrodes were indicated as small black filled circles. The central sulcus and the Sylvian fissure are indicated by white and black dashed lines, respectively. Within the mouth, water, and swallowing, the mainly region where high γ burst was observed were the precentral gyrus, the postcentral gyrus, and the cortex along the Sylvian fissure in each. The β attenuation were observed in wide area related to all three triggers.

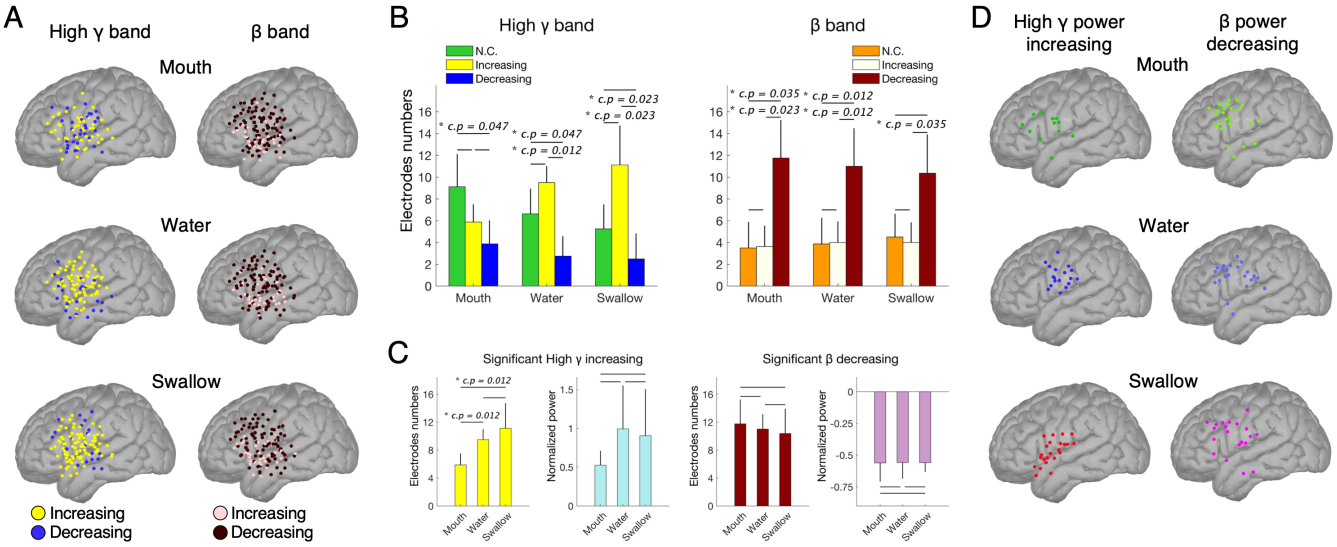

Figure 3. Spatial profile related to mouth, water, and swallowing trigger groups. (A) For each trigger group, electrodes indicating significant power increases or decreases in high γ or β band were plotted over the MNI brain. In the high γ band, a power increase was notable, and in the β band, power decreasing was notable and extensive. (B) Within the mouth, water, and swallowing group, the numbers of electrodes were compared between the three groups including power increasing or power decreasing or no changes (N.C.) (single-sided Wilcoxon signed-rank test). P values were corrected with Bonferroni correction and significant p values (< 0.05) are shown indicated by an asterisk (corrected p: c.p). In the high γ band, the number of increasing electrodes was largest in the swallowing and water groups. In the β band, the number of decreasing electrodes was largest in all groups. (C) In high γ power increasing electrodes or β power decreasing electrodes, the numbers of electrodes and the degree of power changing were compared between the mouth, water, and swallowing group (single-sided Wilcoxon signed-rank test with Bonferroni correction, significant *p* values (< 0.05) are indicated by with an asterisk). The numbers of electrodes with high γ increases associated with mouth were significantly fewer than other groups, but those with β decreased related to mouth were larger than other groups. (D) The top 25% electrodes indicating significant high γ power increases or β decreases were plotted over the MNI brain. In high γ increases, mouth-related electrodes were observed in the precentral gyrus and the ventrolateral prefrontal cortex (VLPFC). Water-related electrodes were observed in the lateral portion of the central sulcus, and swallowing-related electrodes were observed on the regions along the Sylvian fissure. In β decreasing, mouth- and water-related electrodes were localized in the VLPFC, and the localization loosen in the swallowing group. The error bars indicate standard deviation (B, C).

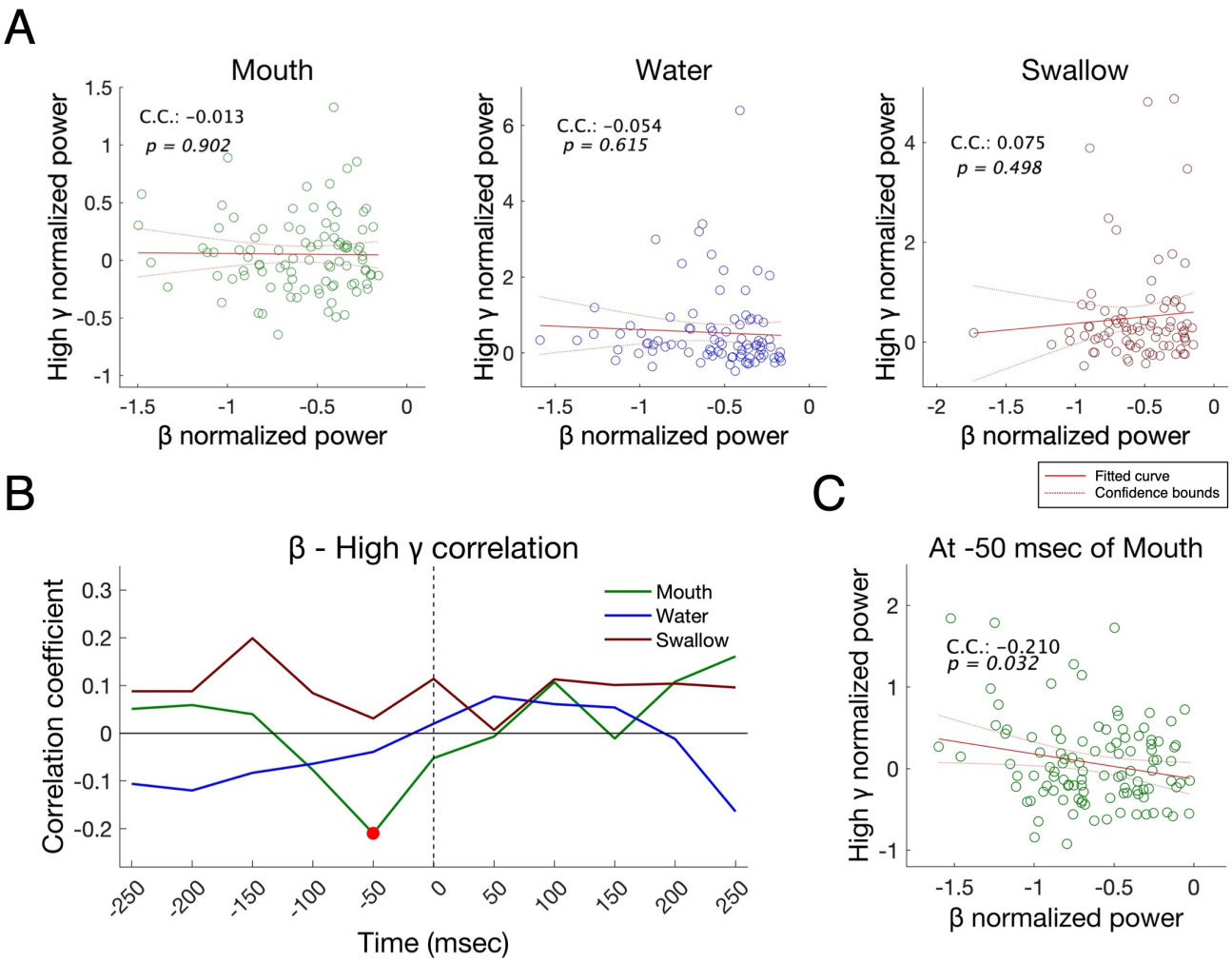

Figure 4. Correlation between β and high γ normalized power within each trigger. (A) Correlation at each trigger of 500 msec time-window are shown. The correlation coefficients (C. C.) were negative in the mouth and water group, and positive in the swallowing group, accompanied with no significant changes. (B) Correlation coefficients between β and high γ normalized power were sequentially plotted from -250 to 250 msec of each trigger. In the mouth group, the significant negative values were observed only at -50 msec indicated as a red circle. (C) Significant negative correlation between β and high γ normalized power at -50 msec were observed (p = 0.032).

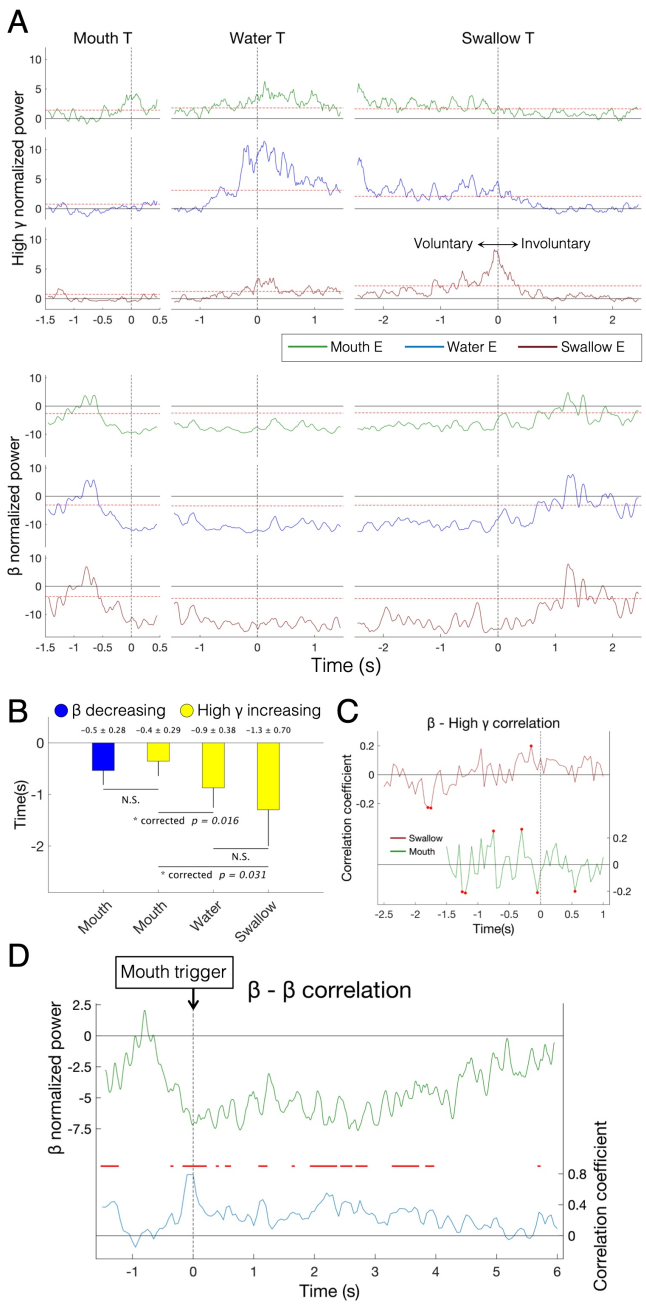

Figure 5. Temporal profile related to swallowing, mouth and water trigger groups. (A) Averaged power of high γ (upper column) and β band (lower column) calculated from top 25% electrodes, which showed significant power changes. The electrodes group which showed top 25% power changes were indicated as Mouth E, Water E, and Swallow E, colored by green, blue, and red in each. At 0 s of mouth triggers (Mouth T), only Mouth E showed a high γ burst not Water E and Swallow E. At 0 s of Water T, Water E showed notably high γ bursts. With Swallow T, Swallow E, showed high γ power increasing and achieved a peak at 0 s. After that, the power decreased. In the β band, three electrodes groups showed the same pattern as the β power decrease from Mouth T, and the attenuation was maintained until about 1.0 s of Swallow T. Red dot lines are FWE-threshold. (B) The beginning time of power changes for each band with each trigger was compared using single-sided Wilcoxon signed-rank test. P values were corrected by Bonferroni correction. The time of the β attenuation and the time of the high γ burst were very similar. The error bars indicate standard deviation. (C) The correlation coefficients between negative β power and high γ power at certain time were plotted with swallowing triggers colored red (upper line) or with mouth triggers colored green (lower line). Significant correlation coefficients ($p < 0.05$) were indicated as red circles. Significant negative correlations were observed at -1.8 s of swallowing triggers and at -1.2 s of mouth triggers. (D) Power changes of β band with mouth triggers from -1.5 s to 6.0 s were presented in upper line, and correlation between β power at -0.05 s and β power at certain time were shown in lower line. During β attenuation, significant positive correlation were observed (corrected $p < 0.05$ with Bonferroni correction, red crossbar indicating significant time).

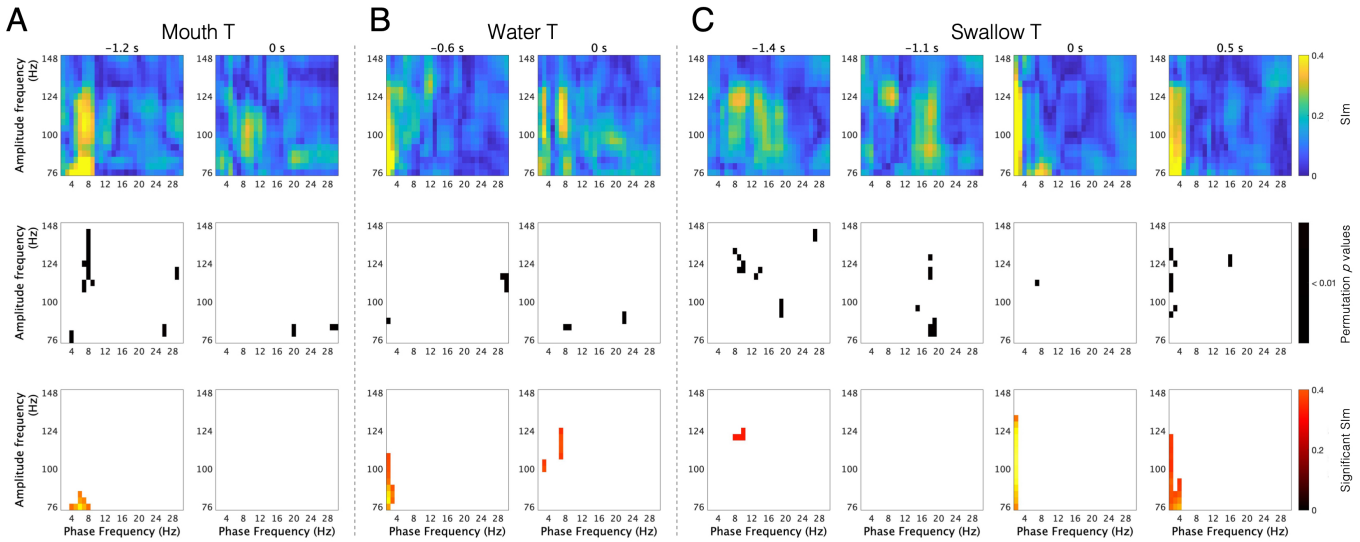

Figure 6. Coupling between the lower frequency phase and the higher frequency amplitude. SIm values were presented in the upper line, permutation p values (boot-strapping technique) less than 0.01 in middle line, significant SIm (FWE-threshold) in bottom line. Vertical axes indicate higher frequency bands (76–150 Hz, 4 Hz bin) from which amplitude were calculated. Horizontal axes indicated lower frequency band (2 – 30 Hz, 1 Hz bin) from which phase were calculated. (A) Coupling between θ (4–8 Hz) and high γ band were observed at -1.2 s of mouth triggers (Mouth T). (B) Related to water T, coupling between δ (2–4 Hz) and high γ band were observed. (C) Coupling between low β (13–20 Hz) and high γ band were observed before 0 s of swallow T, and after 0 s, coupling between δ and high γ band were observed.

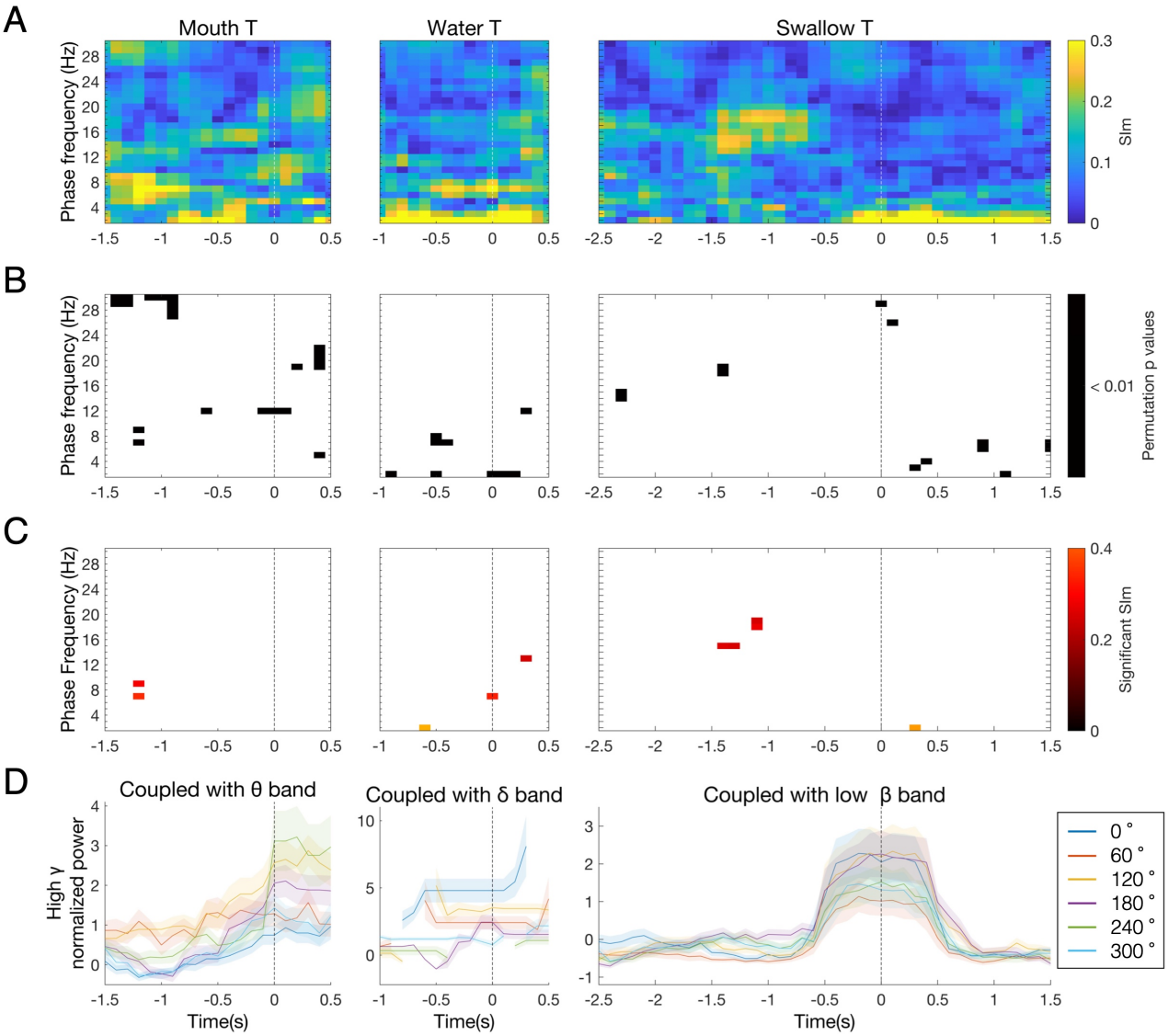

Figure 7. Coupling between lower frequency (2–30 Hz, 1 Hz bin) phase and fixed high γ (75–150 Hz) amplitude. Vertical axes indicated lower frequency band whose phase coupled to high γ amplitude. Horizontal axes indicated the time around each trigger. Values were calculated using 1 s time-window shifted every 100 ms. (A) SIm. (B) Permutation p values (boot-strapping technique) was less than 0.01. (C) Significantly high SIm (FWE-threshold). (D) Phase-condition normalize high γ power were plotted sequentially. From -1.4 s to -0.8 s of mouth T, high SIm between θ (4–8 Hz) and high γ band were observed. From -1.0 s to 0.4 s of water T, high SIm between δ (2–4 Hz) and high γ band were observed. From -1.4 s to -0.7 s of mouth T, high SIm between low β (13–20 Hz) and high γ band were observed. In mouth T and swallow T, the time of high SIm correspond to the time before high γ burst. In water T, the time of high SIm were the time of high γ burst. During observation of high SIm, the phase-conditioned high γ power well separated. The error bars indicate 95% confidence intervals.

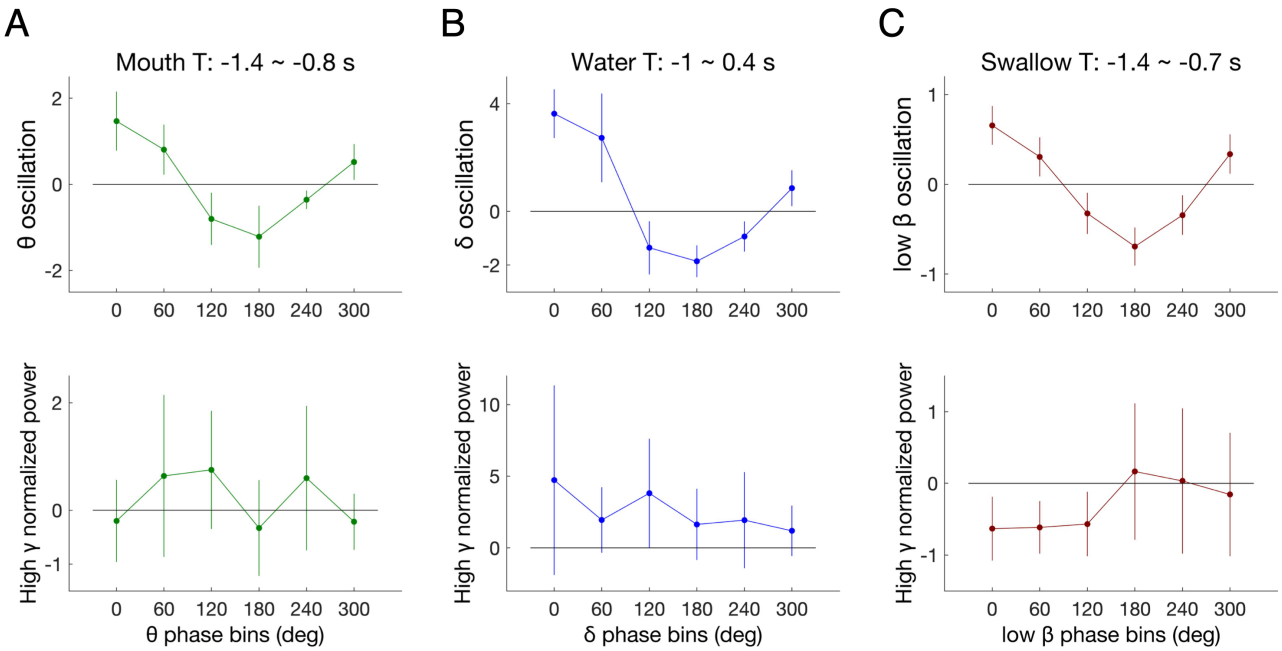

Figure 8. Low-frequency oscillation and high γ (75–150 Hz) power amplitude averaged over each of the 6 phase intervals of low-frequency. In the upper line, specific low-frequency oscillation, θ band (4–8 Hz) with mouth T, δ band (1–4 Hz) with water T and low β band (13–20 Hz) with swallow T, was averaged over each of the 6 phase intervals of the low-frequency oscillation at a specific time when high SIm values were observed. In the lower line, the high-frequency power amplitude, which was conditioned by the low-frequency phases, was averaged over each of the 6 phase intervals of the low-frequency oscillation. (A) During -1.4 s to -0.8 s of mouth T, the lowest power of the high γ was observed at the trough of θ oscillation (180° bin). (B) During -1.0 s to 0.4 s of water T, the largest power of high γ was observed at the peak of δ oscillation (0° bin). (C) During -1.4 s to -0.7 s of swallow T, the largest power of high γ was observed at the trough of low β oscillation (180° bin). The error bars indicate standard deviation.

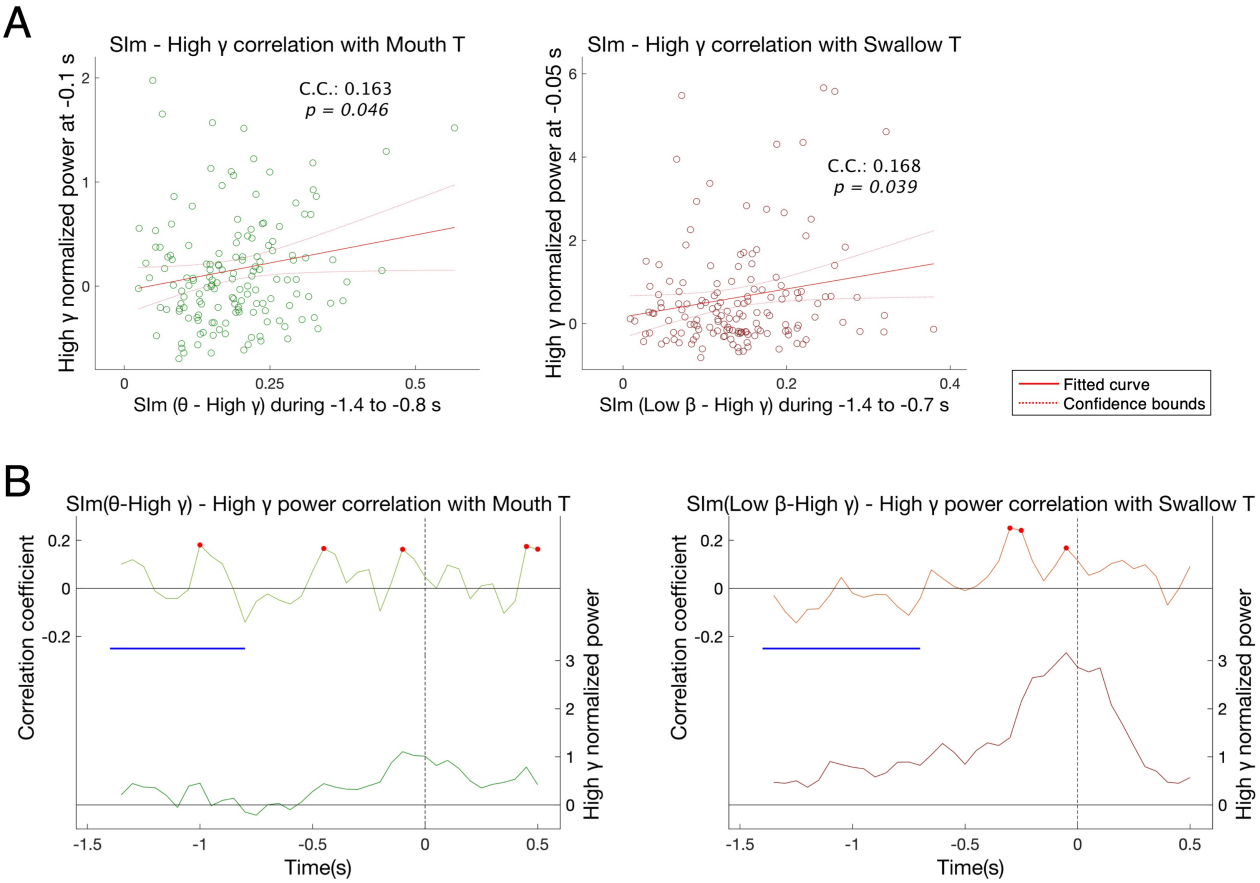

Figure 9. Correlation between fixed SIm and varying high γ normalized power. SIm were calculated from the combination of θ and high γ during -1.4 to -0.8 s of mouth T, low β and high γ during -1.4 to -0.7 s of swallow T. At these time, high SIm values were observed in Fig. 7, and these times are indicated as blue crossbars in Fig. 9B. (A) A significant positive correlation was observed with high γ power at -0.1 s of mouth T (p = 0.046) and with high γ power at -0.05 s of swallow T (p = 0.039). (B) In the upper line, correlation coefficients were sequentially plotted, and in the bottom line, sequential high γ power changes are shown. Significant correlation coefficients are indicated as red circles. Regarding both of mouth T and swallow T, at the time of high γ burst, showed a significant positive correlation.

Supporting Information for

Motor and Sensory Cortical Processing of Neural Oscillatory Activities revealed Human Swallowing using Intracranial Electrodes

Hiroaki Hashimoto, Kazutaka Takahashi, Seiji Kameda, Fumiaki Yoshida, Hitoshi Maezawa, Satoru Oshino, Naoki Tani, Hui Ming Khoo, Takufumi Yanagisawa, Toshiki Yoshimine, Haruhiko Kishima, Masayuki Hirata*

*Masayuki Hirata, M.D., Ph.D.

Email: mhirata@ndr.med.osaka-u.ac.jp

This file includes:

Supporting Figures 1
Supporting Table 1

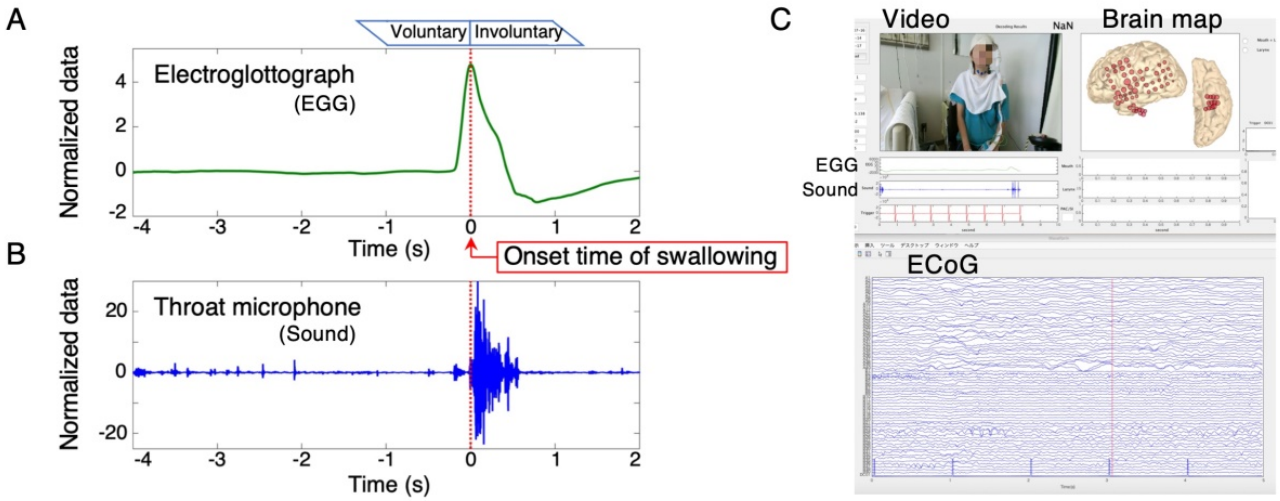

Supporting Figure S1 Across-trials averaged impedance waveforms of an electroglottograph (EGG) (A) and a throat microphone (sound) (B), from one participant (P1) are shown. For analysis, the onset of swallowing was defined as the peak time of an impedance waveform that had been marked as a swallow. (C) The graphical user interface (GUI) we used for synchronizing multimodal data. The GUI, which was originally developed by us as a part of a simple swallow-tracking system (SSTS), shows synchronized multimodal data including the video images, EGG, sound, ECoG waveforms and electrodes brain map.

Clinical profiles

Participant	Age/sex	Diagnosis	Number of Orofacial electrodes (Total Electrodes)	Number of Swallowing Instances	Number of Mouth Openings	Number of Water Injections
P1	36y / F	L TLE	18 (68)	31	31	31
P2	30y / F	L TLE	20 (84)	41	41	41
P3	18y / F	R TLE	18 (55)	27	27	27
P4	24y / M	L TLE	15 (69)	34	34	34
P5	51y / M	L TLE	20 (72)	38	38	38
P6	28y / M	R TLE	20 (96)	27	27	27
P7	20y / M	L TLE	20 (94)	33	33	33
P8	15y / F	L TLE	20 (68)	37	37	37

M, Male; F, Female; R, Right; L, Left; TLE, Temporal lobe epilepsy

Supporting Table S1 Clinical profiles, number of orofacial and total electrodes, and the number of three different triggers for each participant are shown in the table.